

# Experiments of the last 60 years

September 30, 2012

## Contents

1.1	The early years . . . . .	2
1.2	Neutrino experiments . . . . .	3
1.2.1	The Gargamelle experiment . . . . .	3
1.2.2	Underground experiments . . . . .	4
1.2.3	Solar neutrinos . . . . .	4
1.3	High-energy colliding-beam experiments (and some fixed-target results) . . . . .	5
1.3.1	Lepton-nucleon experiments . . . . .	5
1.3.2	Lepton-lepton colliders . . . . .	9
1.3.3	Hadron-hadron colliders . . . . .	12
1.4	Combining results from different colliders . . . . .	13

## 1.1 The early years

Until the 1950s, particle physics was studied by observing cosmic rays in cloud chambers and nuclear emulsion. Around this time, nucleon-nucleon scattering experiments were carried out at cyclotrons and energies became high enough for pions to be produced. Then pion-nucleon scattering was studied. In 1952 Fermi et al. observed



which was a big discovery. Also from electron beams, photons could be made and the reaction



studied although the rate was much lower because of the electromagnetic coupling.

Other processes were also observed :



where the latter is purely leptonic and so provoked large theoretical interest.

In 1956, parity violation in the weak interaction was discovered (predicted by Lee and Yang [1] who received the Nobel Prize). The Wu experiment [2] was the  $\beta$  decay of cobalt-60 nuclei polarised by an external magnetic field, see Fig. 1. The cobalt nuclei are aligned in the magnetic field and are in a state  $J = 5$ . By conservation of angular momentum, as the  $^{60}\text{Ni}^*$  is fixed, the electron and neutrino spins have to be parallel. And as the electron and neutrino are emitted in opposite directions, they have opposite chirality. It was observed that electrons were emitted preferentially opposite to the direction of the magnetic field and not isotropically.

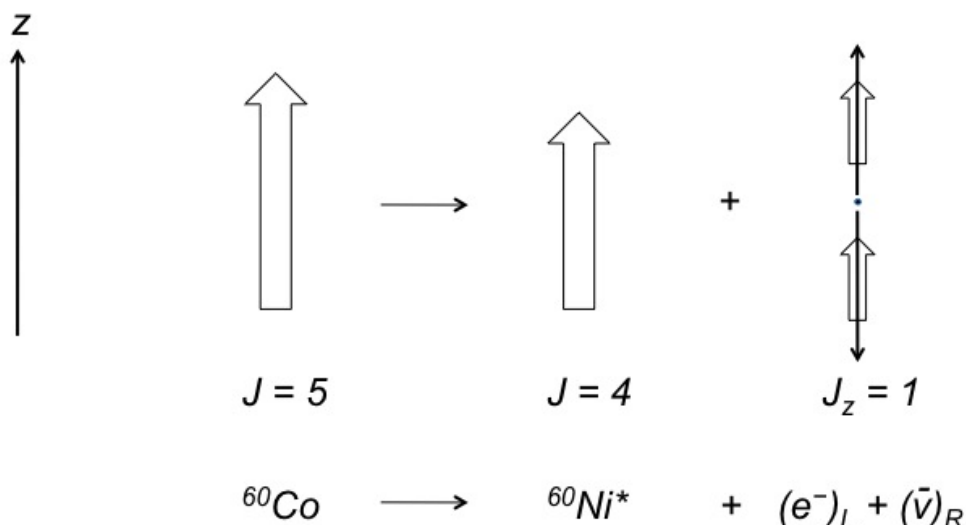


Figure 1: The  $^{60}\text{Co}$  experiment where the electron is emitted preferentially opposite the direction of the spin of the  $^{60}\text{Co}$  nucleus.

During the 1950s and 1960s, large numbers of mesons and baryons were discovered and these were classified into e.g. octets and decuplets depending on their quantum numbers such as

strangeness and isospin. This led to the use of the  $SU(3)$  group to describe these particles [See Symmetries and Conservation Laws course] which accidentally worked as the underlying group, as we now know, is  $SU(3)$ , but this arises from the colours and not the as-know-then three quarks,  $u$ ,  $d$  and  $s$ . These meson classifications can be found in “Particle Physics” by Martin & Shaw.

## 1.2 Neutrino experiments

[Also see course on Neutrino Physics]

### 1.2.1 The Gargamelle experiment

Using the CERN proton synchrotron, protons were extracted from the accelerator and impinged on a thin Beryllium target within a neutrino horn. In the target, pions and kaons were created and the horn partially selected either positive or negative charges. The partially focused  $\pi^+$  decayed to  $\mu^+ + \nu_\mu$ . An iron shield filtered out the remaining hadrons and muons. Measurements of the muons enabled the neutrino spectrum to be determined. Then the neutrinos passed into the large heavy-liquid bubble chamber, Gargamelle. An initial observation of a single electron track coming from it being scattered by a neutrino was the first weak neutral current event. This was unequivocally confirmed by the deep inelastic scattering experiment in which the charge current reaction,

$$\nu_\mu + P \rightarrow \mu^+ + X, \quad (5)$$

as shown schematically in Fig. 2 (left), was expected. This reaction was observed, but the process,

$$\nu_\mu + P \rightarrow \nu_\mu + X, \quad (6)$$

as shown in schematically in Fig. 2 (right), was also seen. This constituted the discovery of neutral currents in 1974 [3].

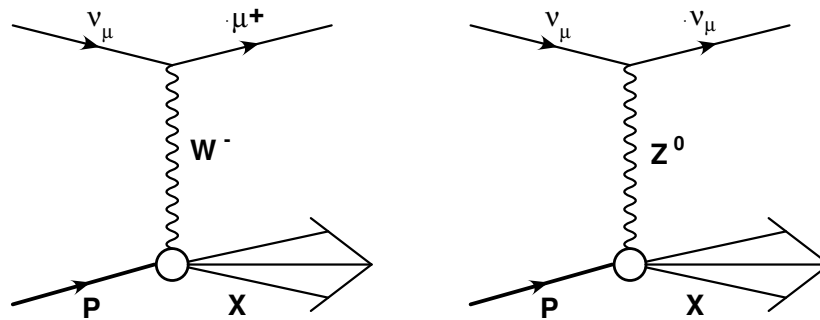


Figure 2: Feynman cartoons of the (left) charge current and (right) neutral current processes for neutrino-proton collisions.

The results, along with electroweak theory, allowed the mass of the  $W$  Boson to be predicted to be  $M_W \sim 70 \text{ GeV}$  which led to the development of the  $S\bar{p}pS$  collider at CERN to search for the mediators of the weak force.

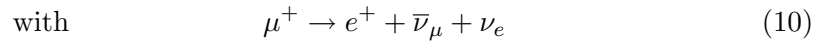
### 1.2.2 Underground experiments

Large underground experiments were built to measure the rate of neutrinos to try and understand such puzzles as the solar neutrino problem as well as looking for proton decay.

- Solar neutrinos are produced primarily by



- Atmospheric neutrinos are produced primarily by proton bombardment of the upper atmosphere



For the production of atmospheric neutrinos, we would crudely expect  $N(\nu_e)/N(\nu_\mu) \sim 1/2$ . This ratio was measured by SuperKamiokande to be closer to 1, demonstrating that muon neutrinos were missing. They also measured an azimuthal variation, i.e.  $N(\nu_\mu)$  versus  $N(\nu_e)$  for neutrinos from the above atmosphere and from the other side of the earth. About half from the other side of the earth were lost suggesting the neutrinos oscillated into  $\nu_\tau$  [4]. With oscillations, this implies that neutrinos have a mass as they must when they have  $v < c$ .

A large detector of water was used to look for :



Both  $\mu^-$  and  $e^-$  were detected by  $\sim 5000$  phototubes by considering their characteristic signals for Cherenkov light. The muon signal rings are sharp whereas those for electrons are more diffuse.

### 1.2.3 Solar neutrinos

In the experiment by Ray Davies [5] mainly “high” energy (14 MeV) neutrinos were used from the process :



They looked for the reaction



for neutrinos impinging on a tank of  $\text{C}_2\text{Cl}_4$ . There were not as many such reactions as was expected in the Standard Model. To detect low-energy neutrinos, tanks of Galium were used

$$\nu_e + \text{Ga} \rightarrow \text{Ge} + e^- . \quad (16)$$

These were also produced at a low rate.

In the Sudbury Neutrino Observatory (SNO), a tank of heavy water ( $\text{D}_2\text{O}$ ) was used to detect the following reaction

$$\nu_e + n \rightarrow e^- + p . \quad (17)$$

Again a deficit of electron neutrinos was seen, 1/3 of that expected [6]. Combined with the Kamiokande results, this explained the solar neutrino problem where we see 1/3 of neutrinos are of electron type and 2/3 oscillate into muon and tau neutrinos. This was further confirmed at SNO when they added salt to the water [7] increasing the sensitivity to  $\nu_\mu$  and  $\nu_\tau$  :

$$\nu_{e/\mu/\tau} + n \rightarrow \nu_{e/\mu/\tau} + n_{\text{scat}} \quad (18)$$

$$\text{then } n + {}^{35}\text{Cl} \rightarrow {}^{36}\text{Cl} + \gamma . \quad (19)$$

This was then consistent with the expected total solar neutrino flux.

The discovery of neutrino oscillations and hence that neutrinos have mass was in contradiction to expectations from the Standard Model. This is the only example of the Standard Model being proven wrong, hence the increased interest in neutrino experiments over the last 10 years or so. Further neutrino oscillation experiments are ongoing at reactors (source of copious low-energy neutrinos from  $\beta$  decay) and at accelerators, such as MINOS and T2K. These have recently measured  $\theta_{13}$  to be non-zero and quite large (see results from Daya Bay and RENO in particular).

### 1.3 High-energy colliding-beam experiments (and some fixed-target results)

There are various different types of colliding beams which have different properties and can probe different phenomena. Some experiments/colliders are dedicated (e.g. Belle/Babar or lepton-flavour violation,  $\mu \rightarrow e$ , etc.) or multi-purpose (e.g. LHC, LEP, etc.). Can classify colliders into three types :

1.  $e^+e^-$  : this is purely leptonic, is therefore clean and has a controlled centre-of-mass energy. It has a large discovery potential as well as precision physics. Limited by synchrotron radiation, so need to consider linear colliders.
2.  $NN(PP)$  : highest energy and large discovery potential. Messy.
3.  $lN$  : Mixture of the two. One probe and one structured object.

#### 1.3.1 Lepton-nucleon experiments

In the period 1950–70, deep inelastic scattering experiments using  $e^-$ ,  $\nu$  and  $\mu$  beams were used to probe the structure of the proton and neutron. In particular, pioneering experiments at SLAC (Hofstadter et al. [8]) measured the size of the proton ( $\sim 10^{-13}$  m) with indications of a substructure which was measured in subsequent experiments. The results suggested that scattering occurred off point-like objects in the nucleon and  $\sim 50\%$  of the nucleon interacted in this way. The remaining 50% was carried by the gluons. This was the beginning of QCD.

At HERA, this has been advanced further in  $eP$  collisions. Electrons (or positrons) at 27.5 GeV collided with protons of 920 GeV, yielding a centre-of-mass energy of about 320 GeV. There were two multi-purpose detectors which measured a wide range of phenomena : proton and photon structure; other aspects of QCD; electroweak physics; and searches for beyond the Standard Model (e.g. leptoquarks).

We will here discuss two closely related measurements. Firstly the structure of the proton which has been measured over a vast kinematic range compared to the first measurements in the 1960s. The basic process is shown in Fig. 3 (left), where a neutral current (a neutral propagator) process results in the electron scattering in the detector and a photon with squared four-momentum,  $Q^2$ , exchanged. This is essentially related to the wavelength of the probe, i.e. high  $Q^2$  implies a high resolving power. The other relevant variable is the proton's momentum fraction,  $x$ , carried by the struck quark. This can be visualised in Fig. 4, where the struck quark has a momentum,  $xp$ .

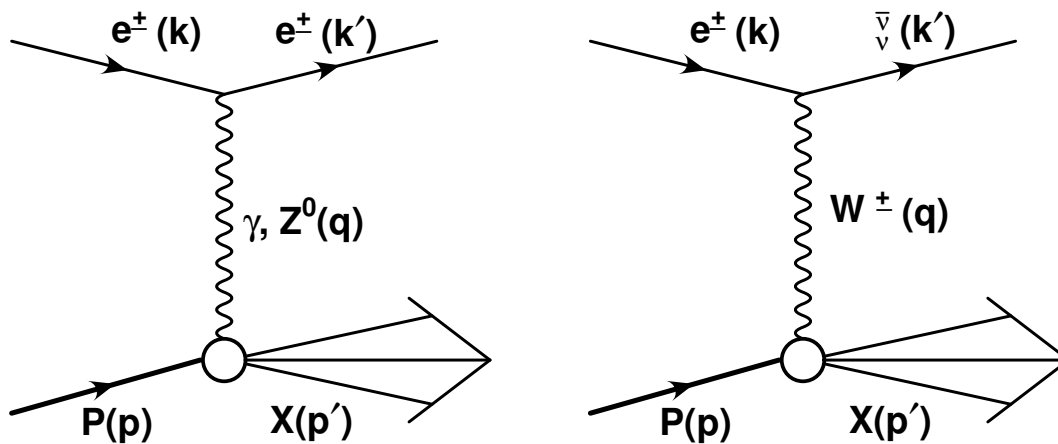


Figure 3: Feynman cartoons of (left) neutral current and (right) charge current  $eP$  scattering.

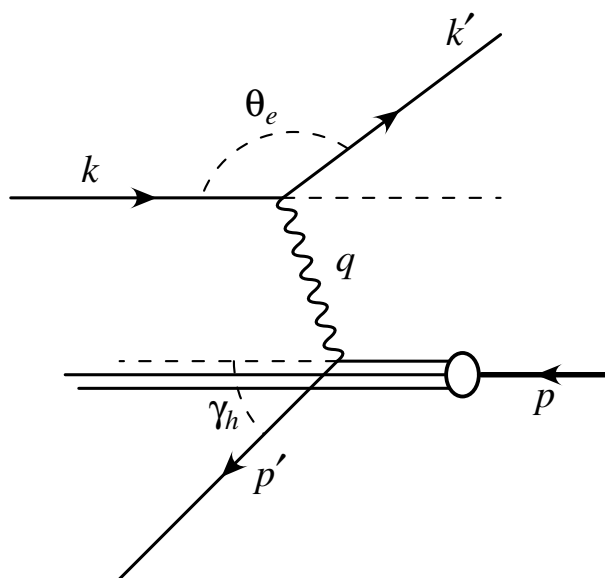


Figure 4: More detailed Feynman cartoon of  $eP$  deep inelastic scattering and its kinematics.

Figure 5 shows the cross section for deep inelastic scattering versus  $Q^2$  for different fixed values of  $x$  for the HERA data as well as the earlier fixed-target data. The region of high  $x$  probes

the quark densities in the the proton and low  $x$  probes the gluon density. Overall, this gives us precise knowledge of the structure of matter, one of the fundamental goals of physics. Also, practically, such knowledge is needed by current colliders which use protons (e.g. LHC) so that you know what you are colliding.

## H1 and ZEUS

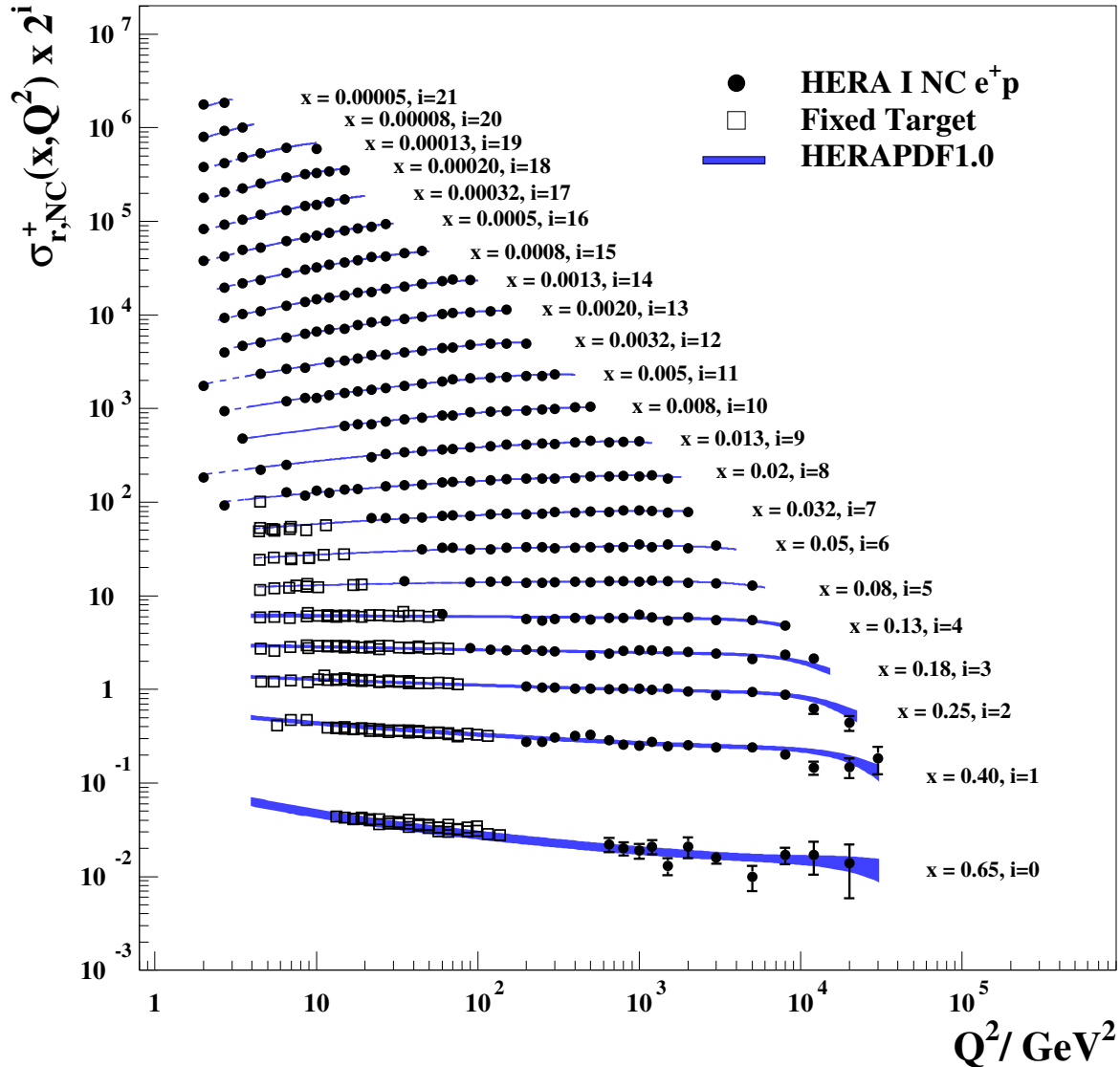


Figure 5: Cross section for neutral current deep inelastic scattering versus the virtuality,  $Q^2$ , at different values of  $x$ . From [9].

Another classic measurement made at HERA [10] is shown in Fig. 6 in which the neutral current cross section was measured at high  $Q^2$  and also the charge current (see Fig. 3 (right)) cross section. At low  $Q^2$ , the neutral current cross section is dominated by photon exchange which is very much higher than the charge current cross section. The cross sections for the two process are, however, observed to unify at  $Q^2 \sim M_{W,Z}^2 \sim 10^4 \text{ GeV}^2$ .

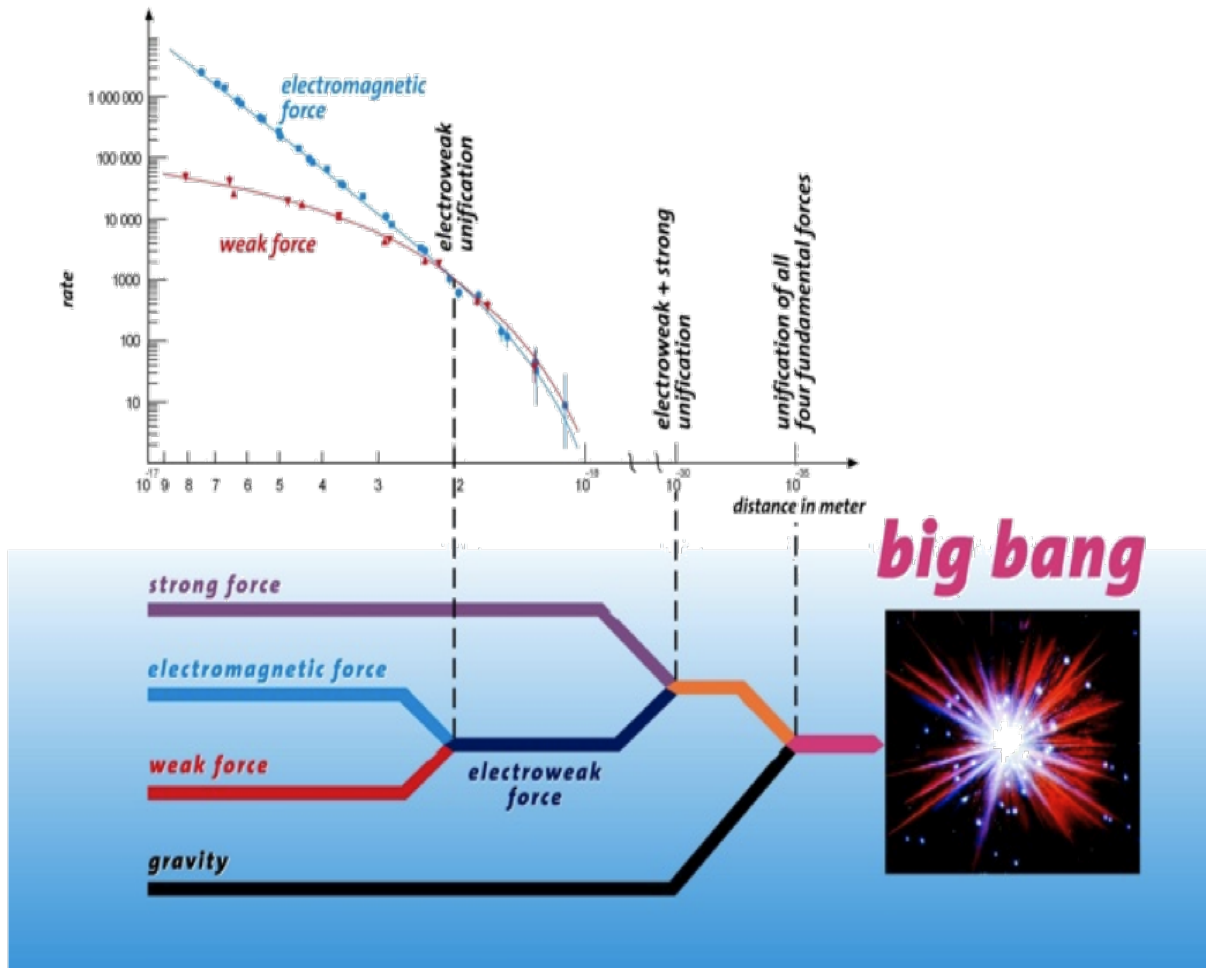


Figure 6: Measurements of neutral current (electromagnetic force) and charge current (weak force) cross sections at HERA demonstrating the scale at which the forces unify. Note the scale for unification with the strong force and gravity. Although a schematic, (publicity plot) the data are the real HERA measurements, here shown as a function of distance but usually plotted versus the scale,  $Q^2$ , with the point of unification at about  $Q^2 \sim M_{W,Z}^2 \sim 10^4 \text{ GeV}^2$ .

### 1.3.2 Lepton-lepton colliders

There have been a multitude of  $e^+e^-$  experiments with a centre-of-mass energy of a few to over 200 GeV. There is planning for a linear  $e^+e^-$  collider of  $\mathcal{O}$  (TeV). Some highlights.

The charm quark was discovered in 1974 at SLAC [11] and  $P+Be$  at BNL [12] via the detection of the decay of the bound state, the  $J/\psi$  meson, to a pair of muons,  $M_{J/\psi} \sim 3.1$  GeV. A scan of the  $e^+e^-$  total cross section, Fig. 7, shows how discoveries were made and why collider beam energies can be chosen.

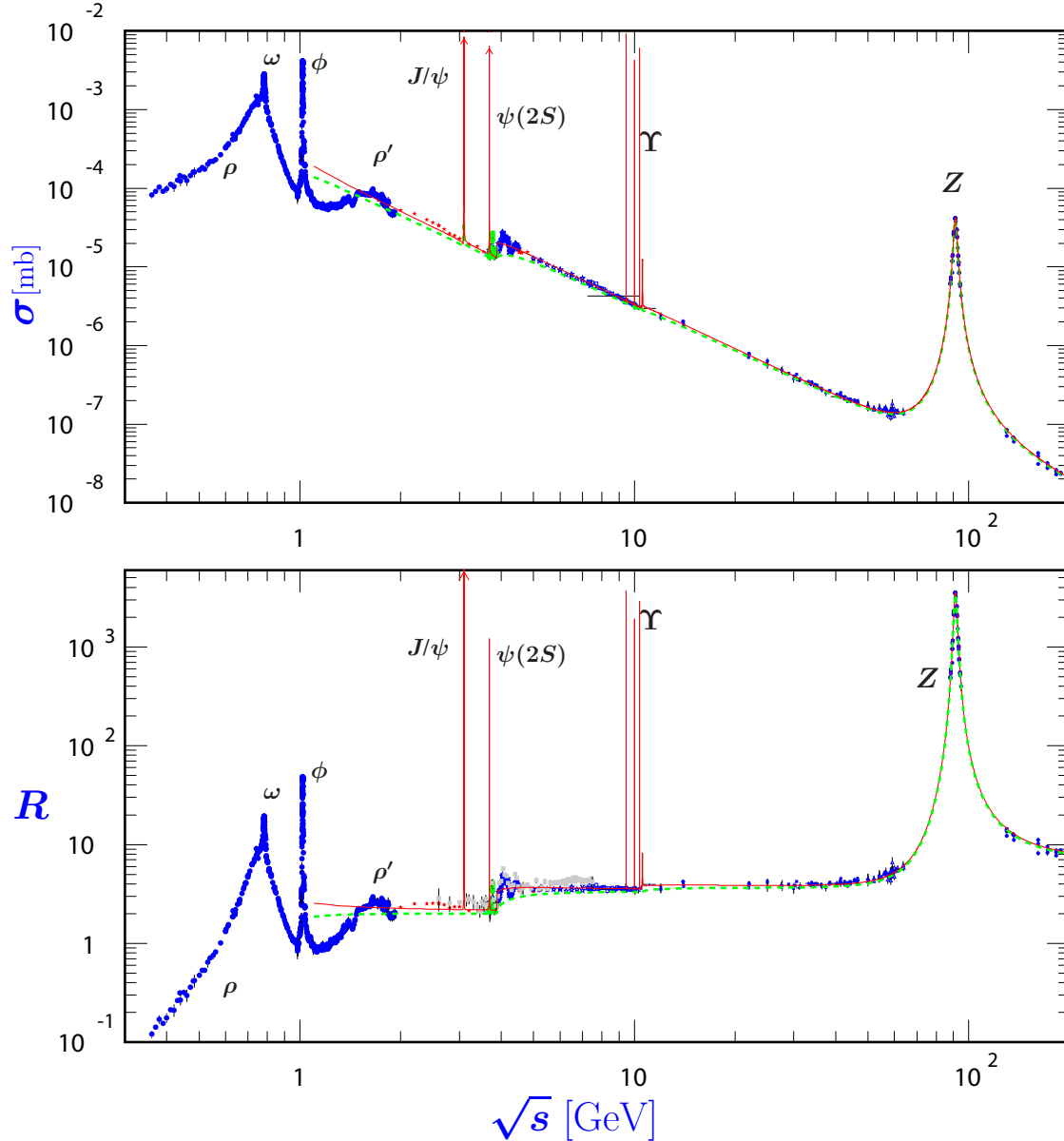


Figure 7: Measurement of the total cross section,  $e^+e^- \rightarrow \text{hadrons}$ , and ratio,  $e^+e^- \rightarrow \text{hadrons}/e^+e^- \rightarrow \mu^+\mu^-$ , as a function of the centre-of-mass energy,  $\sqrt{s}$ . The curves are a guide using simple theoretical models. From [14].

In 1979, the gluon was discovered [13] by the experiments at the PETRA collider in DESY with  $\sqrt{s} = 35$  GeV. Although electron-positron collisions are a clean leptonic environment, they can be powerful probes of QCD. The gluon was discovered through the observation of three-jet

events. Most simply, one would expect two jets to be produced of equal energy and back-to-back as shown schematically in Fig. 8 (left). However, in the detector, three jets (see schematic in Fig. 8 (right)) were observed where one of the quarks had radiated a gluon.

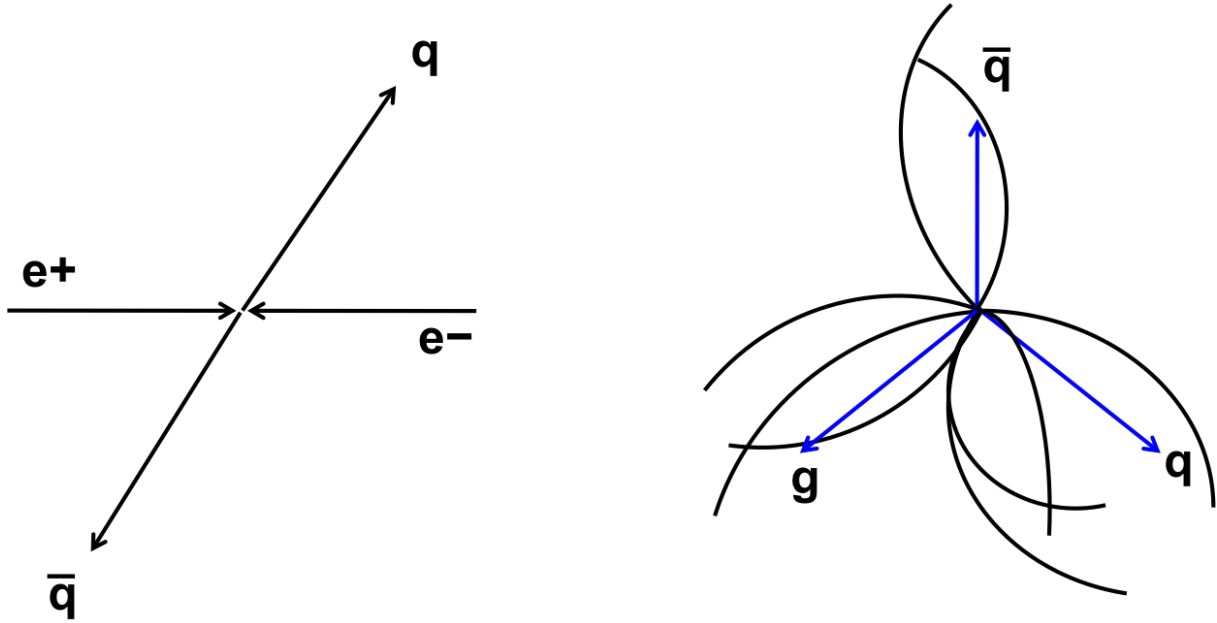


Figure 8: (Left) schematic of an  $e^+e^-$  collision in which a quark and anti-quark are produced back-to-back. (Right) Additional events observed in which a star-like, three-jet, configuration was seen, consistent with the additional production of a gluon.

In 1989, the Large Electron-Positron (LEP) collider turned on embarking (along with SLD, a linear collider running at  $\sqrt{s} \sim M_Z$ ) on a new era of precision physics. Initial LEP running was at the  $Z$  peak,  $\sim 91$  GeV, then moved through  $2M_W \sim 160$  GeV and finally up to just over 200 GeV, looking for the Higgs Boson. There were four multi-purpose experiments which were most famous for precision measurements of electroweak parameters such as  $M_Z$  and  $M_W$ . The measurement of the cross section as a function of  $\sqrt{s}$  was fundamental in measuring  $M_Z$  and constraining the number of neutrinos, see Fig. 9.

The values for  $M_Z$  and  $M_W$  are [14] :

$$M_Z = 91.1876 \pm 0.0021 \text{ GeV} \quad (20)$$

$$M_W = 80.385 \pm 0.015 \text{ GeV} \quad (21)$$

where the latter is still being improved by the Tevatron. In the absence of direct measurements, precise determinations of known parameters constrain new physics phenomena, e.g. the mass of the Higgs Boson. In its final throws, LEP also searched for the Higgs, via Higgsstrahlung (see Fig. 10), where a virtual  $Z$  results in a real  $Z$  and a Higgs Boson. The centre-of-mass energy was constantly cranked up as  $\sqrt{s} > M_H + M_Z$  is required.

Limits of circular  $e^+e^-$  machines are being reached due to the rate of energy loss due to synchrotron radiation. The next planned major collider is the International Linear Collider (ILC). This would complement the LHC because of the precisely controlled initial state and cleaner final states. It could also act as a “factory” for e.g.  $t\bar{t}$  production, Higgsstrahlung or pair production of exotic particles.

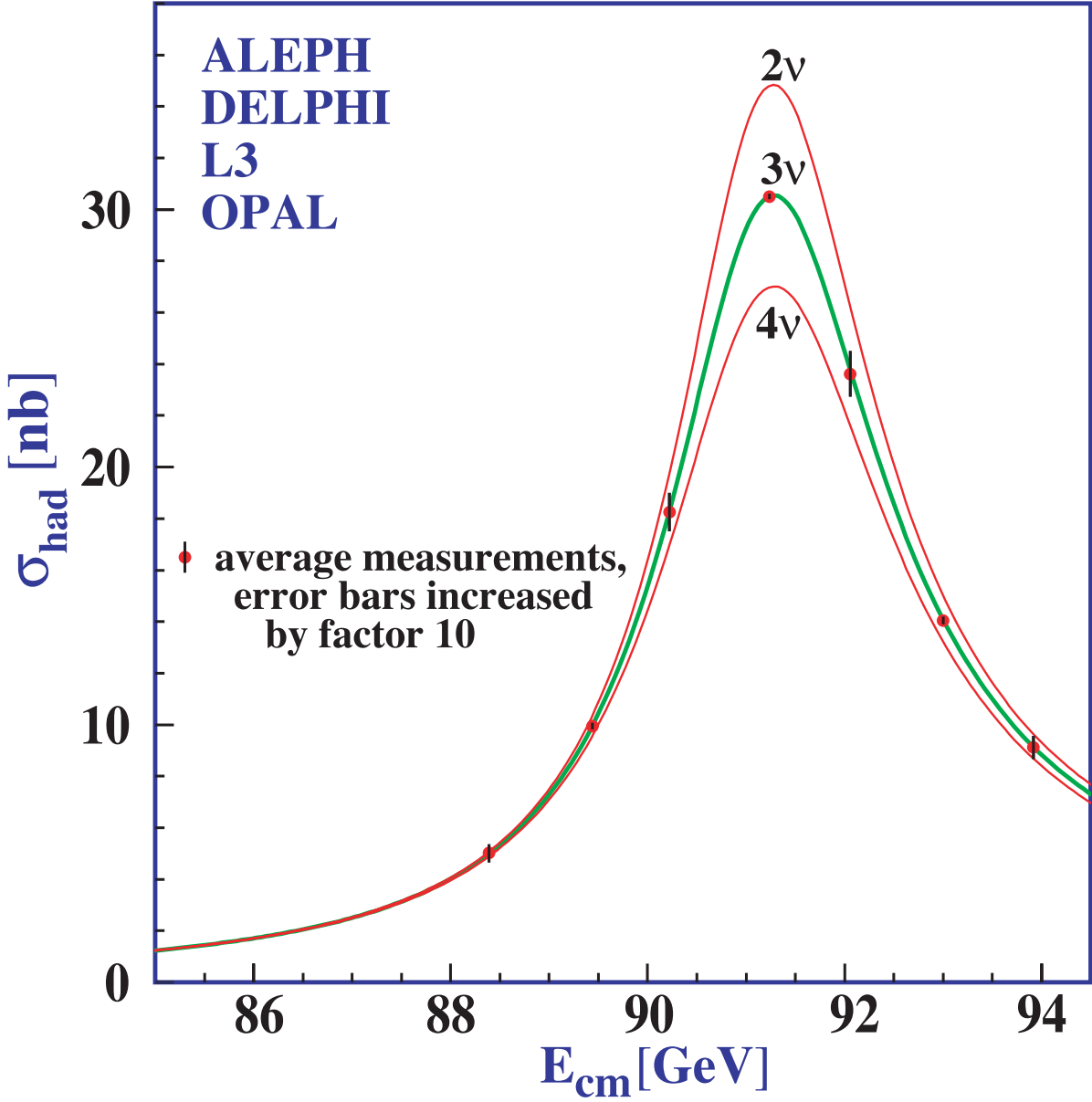


Figure 9: Combined LEP data on the cross section,  $e^+e^- \rightarrow \text{hadrons}$ , as a function of centre-of-mass energy near  $M_Z$ . The curves show the predictions of the Standard Model with two, three, and four species of light neutrinos. The asymmetry of the curve is produced by initial-state radiation. Note that the error bars have been increased by a factor ten for display purposes. From [14, 15].

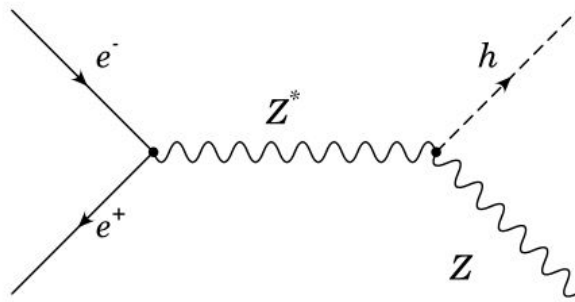


Figure 10: Feynman diagram for the Higgsstrahlung process, in which a virtual  $Z$  radiates a Higgs Boson, accompanied by a real  $Z$ .

### 1.3.3 Hadron-hadron colliders

Due to hadronic structure and multitude of final states, these are more complex than  $e^+e^-$  colliders. But they are usually at the energy frontier and thereby produce discoveries and measurements of known phenomena over a large kinematic range. Some of the major results are as follows.

The total cross section for a hadron collision, see Fig. 11, does not have such a rich structure as for the  $e^+e^-$  result, although at lower energies resonances can be seen. This also has relevance for building detectors and particle interaction in matter.

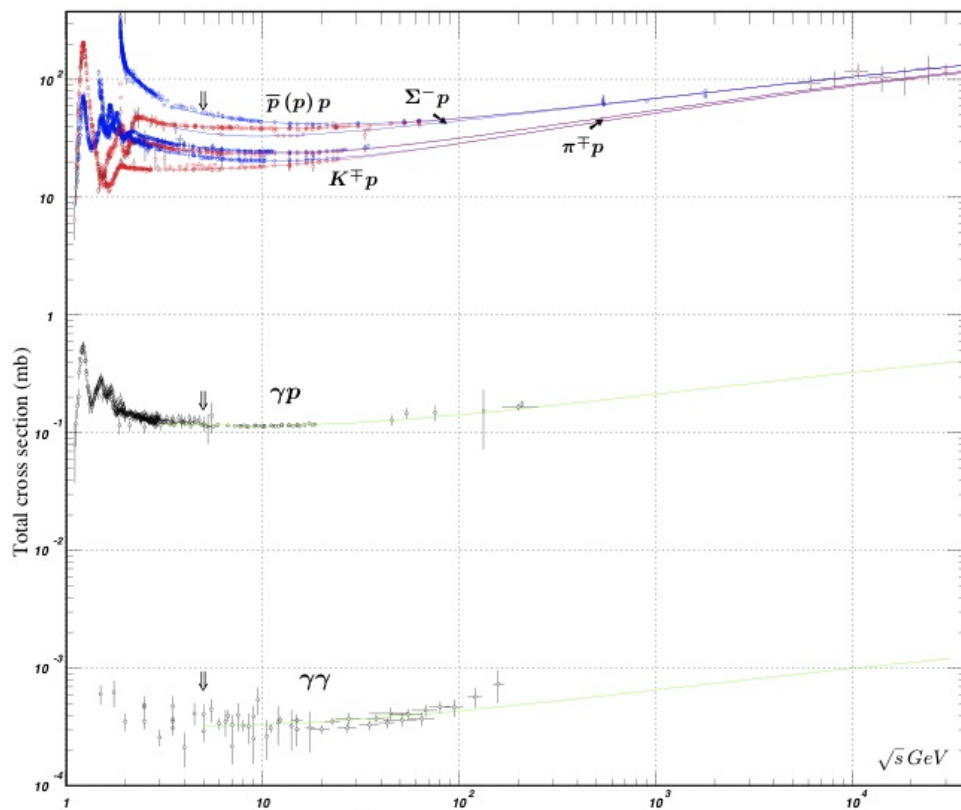


Figure 11: Total cross section for various hadron collisions. From [14].

The bottom quark was discovered [16] in 1977 by production of  $\Upsilon$  mesons decaying into a pair

of muons in  $p$ Be collisions at Fermilab. As is often the case for discoveries, this was seen in the spectrum of the invariant mass of the muon pair, see Fig. 12, with a clear resonance structure observed.

The  $W$  and  $Z$  bosons were discovered in the early 1980s [17] at the  $S\bar{p}p$ S collider at CERN,  $\sqrt{s} = 540$  GeV. The leptonic decays of the  $W$  and  $Z$  were measured as these have relatively low backgrounds compared to hadronic channels. Similarly, the top quark was discovered by CDF and D0 [18] at  $\sqrt{s} = 1800$  GeV in 1995.

Not a discovery, but a measurement which can lead to such and has a lot of physics, examples of which are shown in Figs. 13 and 14, is the inclusive jet cross section. This distribution which falls over many orders of magnitudes probes the highest scales and could reveal new physics, e.g. quark substructure, and provides a powerful test of QCD.

## 1.4 Combining results from different colliders

Combining results from different colliders can simply benefit a measurement by increasing the precision (cf.  $M_W$ ) or providing an independent cross-check (cf. discovery of the  $J/\psi$ ). Before these can be done, one has to check that the physics at the different colliders is the same, a far from trivial question. An example is the universality of fragmentation which states that the final state process of fragmentation (or hadronisation) is independent of the initial particle, e.g. if the available energy at collision is the same, then the momentum spectrum of the produced particles does not depend on the flavour of collision. Figure 15 shows [14, 20] the scaled momentum and that the trends seen in  $e^+e^-$  and  $ep$  collisions are the same. This relies on the concept of factorisation in which parts of the process, e.g. the hard scatter and fragmentation, can be split into two parts and e.g. the factorisation is universal.

The result of combining different data measuring the strong coupling,  $\alpha_s$ , is shown in Fig. 16. The different sets of data provide extra precision, some have a wider kinematic range and so test the “running” more rigorously. The data are not only from different colliders but measure completely different processes, e.g. jet cross sections,  $\tau$  decays, electroweak fits, etc.. This has led to a precision of 0.6%.

One of the primary reasons for measuring  $\alpha_s$  to increased precision is to predict the point of when the weak, strong and electromagnetic forces unify. Given their current precision and their expected evolution with energy, the three forces will not unify at any scale, see Fig. 17 (left). Inclusion of a model of Supersymmetry which modifies the evolution of couplings “solves” this problem, see Fig. 17 (right).

Finally, the “holy grail” of particle physics is the search for the Higgs Boson. As discussed before, LEP ruled this out for masses below about 114 GeV. Recently, the ATLAS [22] and CMS experiments [23] have both discovered a new particle which looks like a Higgs Boson with a mass of about 125 GeV [indications have also been seen by the Tevatron experiments]. Both LHC experiments have published signals of about  $6\sigma$ , combining various channels, see Fig. 18.

## References

- [1] T.D. Lee and C.N. Yang, Phys. Rev. **104** (1956) 254.
- [2] C.S. Wu et al., Phys. Rev. **105** (1957) 1413.
- [3] F.J. Hasert et al., Phys. Lett. **46** (1973) 121;  
F.J. Hasert et al., Phys. Lett. **46** (1973) 138.
- [4] SuperKamiokande Collaboration, Phys. Rev. Lett. **86** (2001) 5651;  
SuperKamiokande Collaboration, Phys. Lett. **B 539** (2002) 179.

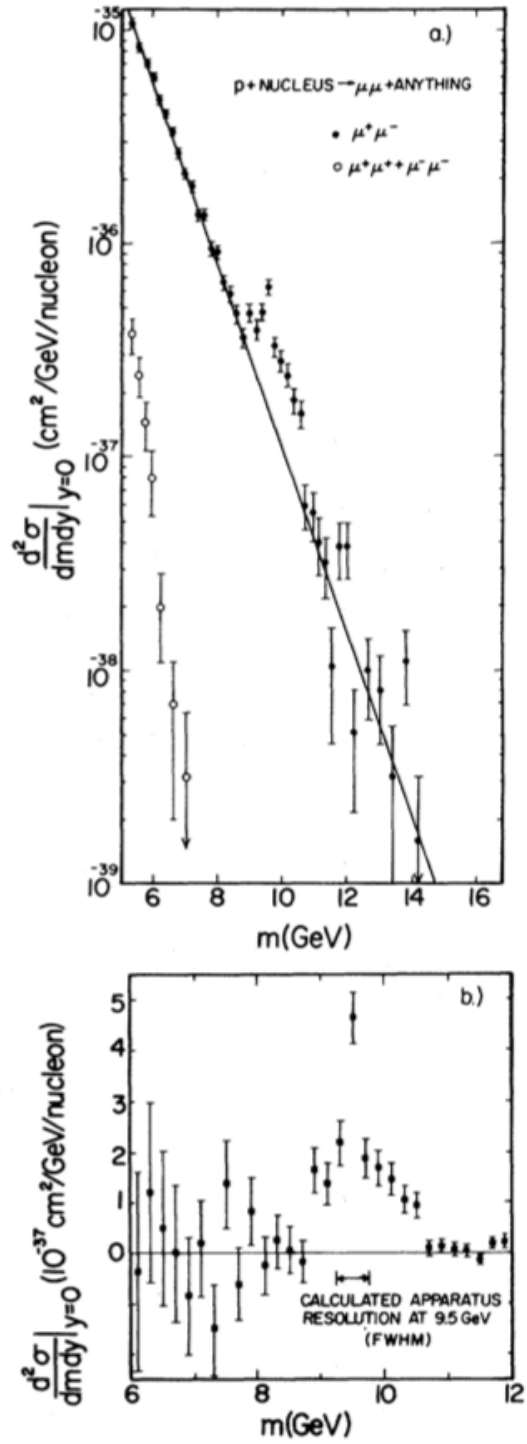


Figure 12: Distribution of Invariant mass of pairs of muons, showing clear enhancement above the continuum at about 9.5 GeV. From [16].

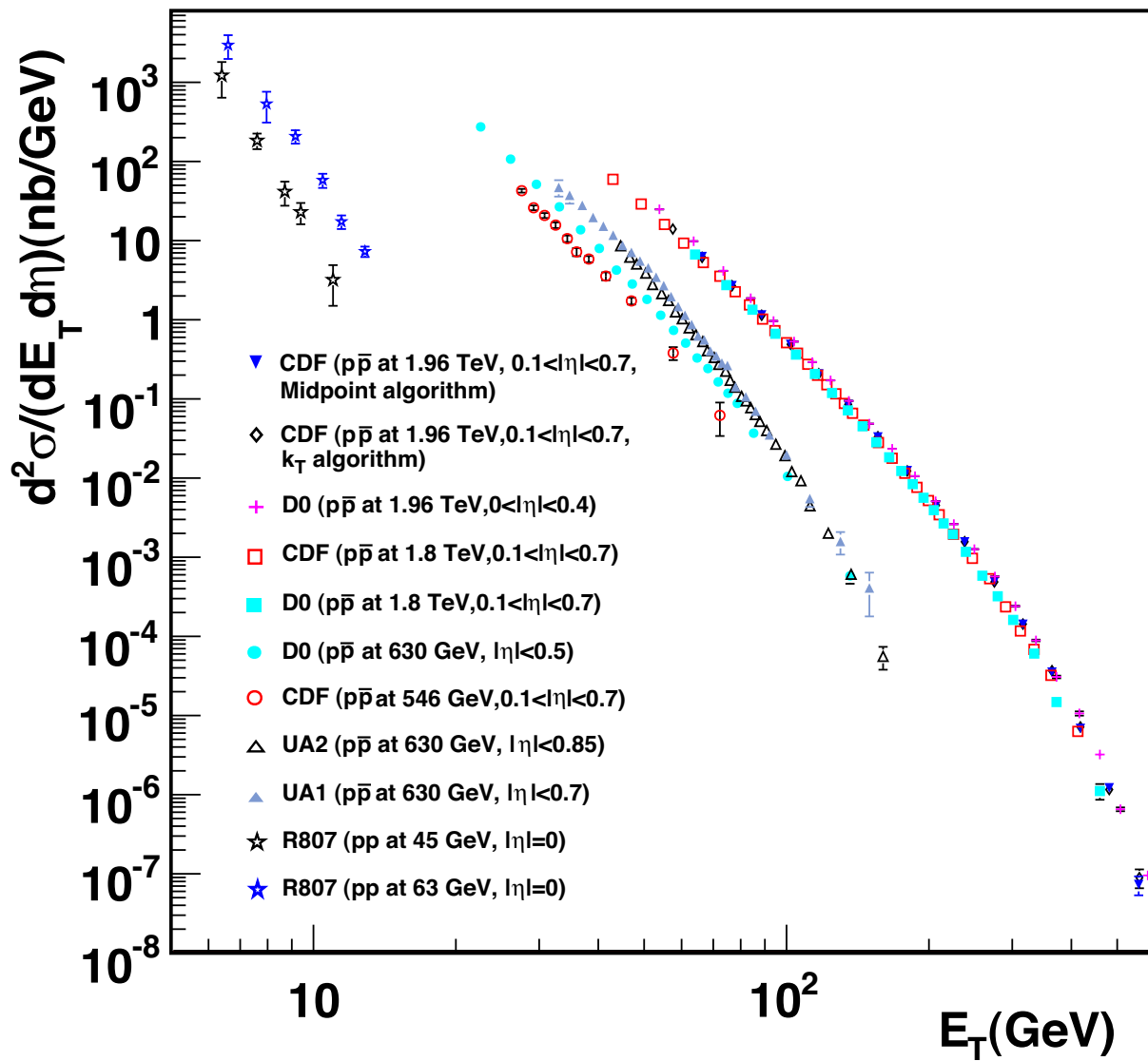


Figure 13: Inclusive jet cross section (pre-LHC) as a function of jet  $p_T$ . From [14].

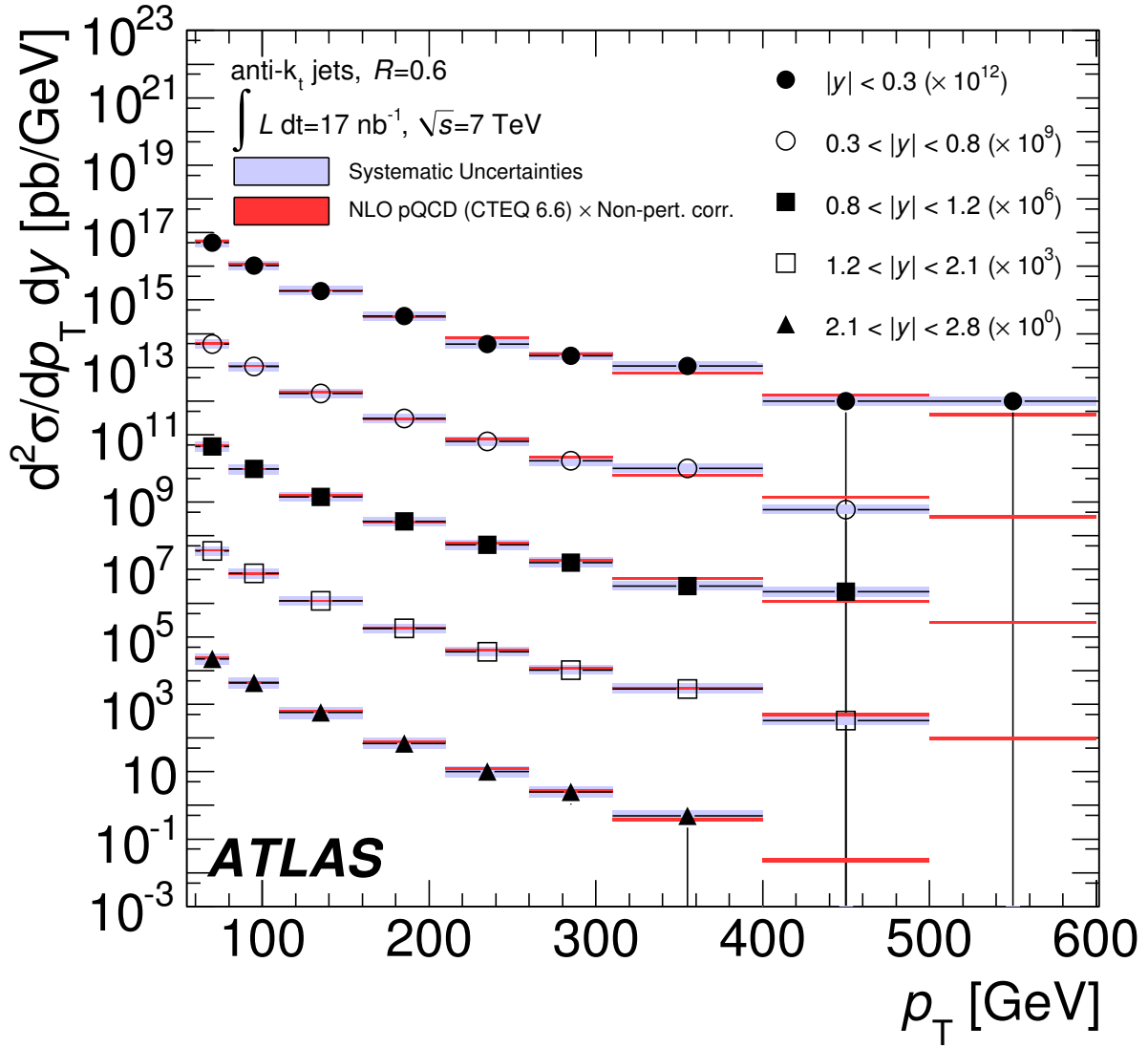


Figure 14: Inclusive jet double-differential cross section as a function of jet  $p_T$  in different regions of rapidity. From [19].

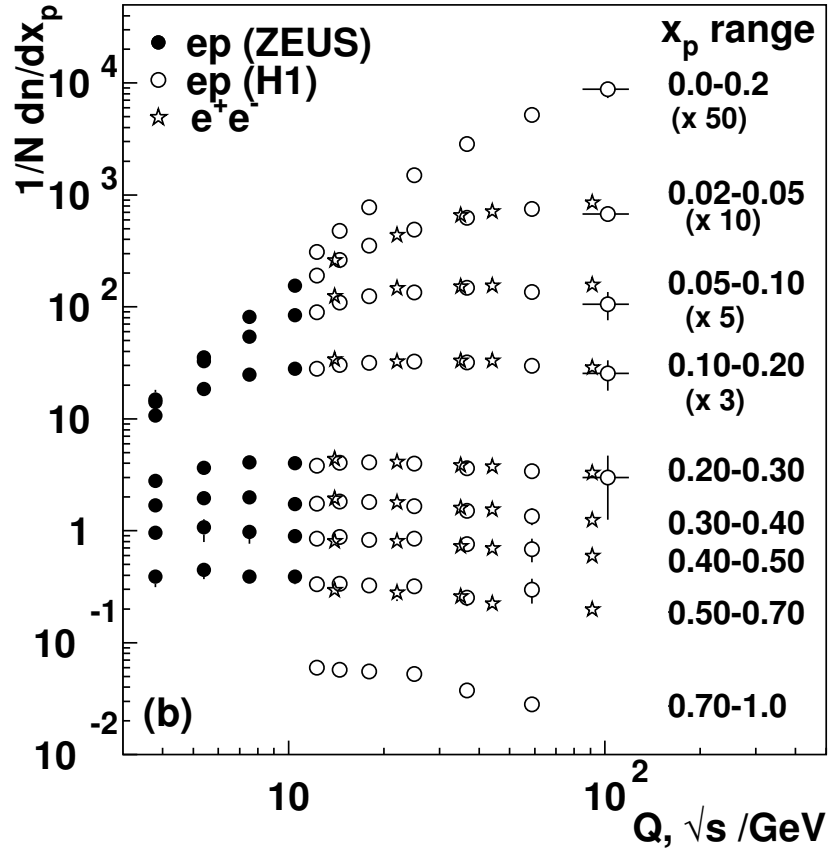


Figure 15: Scaling violations of the fragmentation function for all charged particles in deep inelastic scattering and  $e^+e^-$  interactions. From [14].

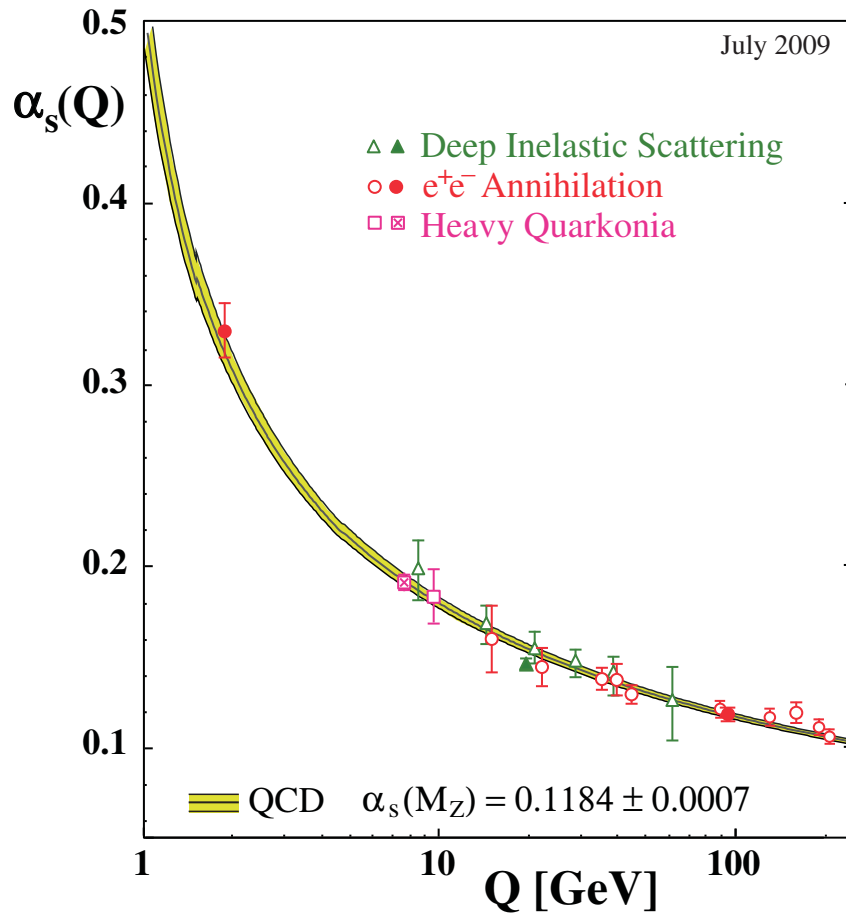


Figure 16: Compilation of measurements of the strong coupling,  $\alpha_s$ , versus the scale of the interaction. From [21].

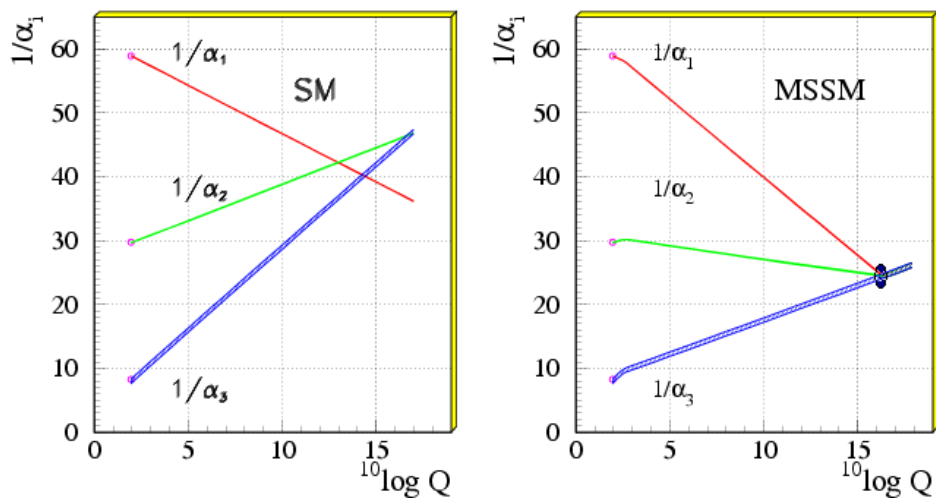


Figure 17: Gauge coupling unification in non-SUSY GUTs on the left versus SUSY GUTs on the right using the LEP data as of 1991. From [24].

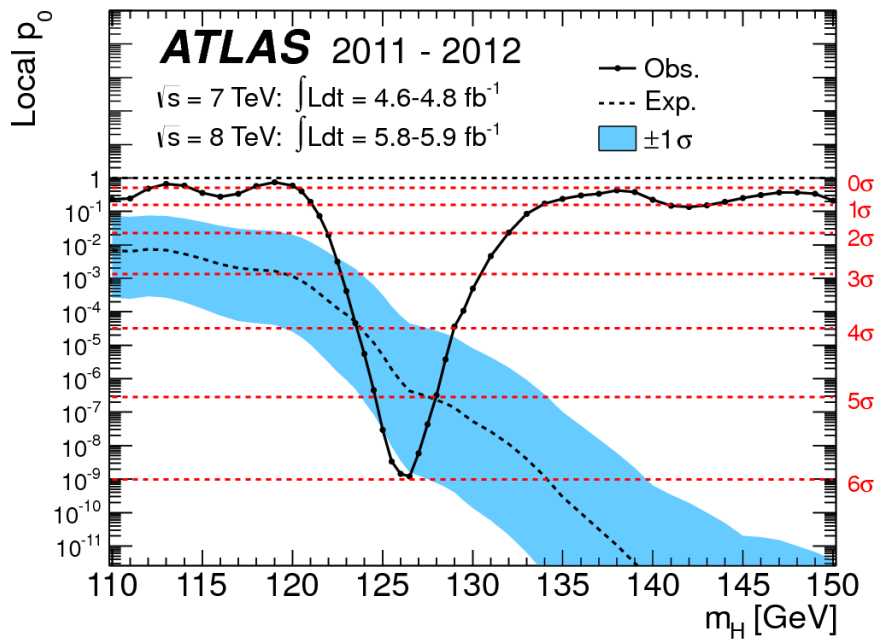


Figure 18: Limit on Higgs Boson from ATLAS as of August 2011. From [22].

- [5] R. Davis, D.S. Harmer and K.C. Hoffman, Phys. Rev. Lett. **20** (1968) 1205.
- [6] SNO Collaboration, Phys. Rev. Lett. **87** (2001) 071301; SNO Collaboration, Phys. Rev. Lett. **89** (2002) 011301;
- [7] SNO Collaboration, Phys. Rev. Lett. **92** (2004) 181301.
- [8] R. Hofstadter, H.R. Fechter and J.A. McIntyre, Phys. Rev. **92** (1953) 978.
- [9] H1 and ZEUS Collaborations, JHEP **1** (2010) 1.
- [10] Several papers go into this plot. As examples of such measurements, see  
 ZEUS Collaboration, Euro. Phys. J. **C 70** (2010) 945;  
 H1 Collaboration, Euro. Phys. J. **C 19** (2001) 269.
- [11] J.-E. Augustin et al., Phys. Rev. Lett. **33** (1974) 1406.
- [12] J.J. Aubert et al., Phys. Rev. Lett. **33** (1974) 1404.
- [13] JADE Collaboration, Phys. Lett. **B 91** (1980) 142;  
 JADE Collaboration, Phys. Lett. **B 101** (1981) 129;  
 MARK J Collaboration, Phys. Rev. Lett. **43** (1979) 830;  
 MARK J Collaboration, Phys. Rev. Lett. **50** (1983) 2051;  
 PLUTO Collaboration, Phys. Lett. **B 86** (1979) 418;  
 PLUTO Collaboration, Z. Phys. **C 28** (1985) 365;  
 TASSO Collaboration, Phys. Lett. **B 86** (1979) 243;  
 TASSO Collaboration, Phys. Lett. **B 97** (1980) 453.
- [14] K. Nakamura et al. (Particle Data Group), J. Phys. **G 37** (2010) 075021; and 2011 partial update for the 2012 edition. <http://pdgl.b1.gov>
- [15] ALEPH Collaboration, Euro. Phys. J. **C 14** (2000) 1;  
 DELPHI Collaboration, Euro. Phys. J. **C 16** (2000) 371;  
 L3 Collaboration, Euro. Phys. J. **C 16** (2000) 1;  
 OPAL Collaboration, Euro. Phys. J. **C 19** (2001) 587;  
 The ALEPH, DELPHI, L3, OPAL, SLD Collaborations, Phys. Rept. **427** (2006) 257.
- [16] S.W. Herb et al., Phys. Rev. Lett. **39** (1977) 252.
- [17] UA1 Collaboration, Phys. Lett. **B 107** (1981) 320;  
 UA1 Collaboration, Phys. Lett. **B 122** (1983) 103;

- UA1 Collaboration, Phys. Lett. **B 126** (1983) 398;  
UA2 Collaboration, Phys. Lett. **B 122** (1983) 476;  
UA2 collaboration, Phys. Lett. **B 129** (1983) 130.
- [18] CDF Collaboration, Phys. Rev. Lett. **74** (1995) 2626; D0 Collaboration, Phys. Rev. Lett. **74** (1995) 2632;
- [19] ATLAS Collaboration, Euro. Phys. J. **C 71** (2011) 1512.
- [20] TASSO Collaboration, Z. Phys. **C 47** (1990) 187;  
ZEUS Collaboration, Phys. Lett. **B 414** (1997) 428;  
H1 Collaboration, Phys. Lett. **B 654** (2007) 148;  
DELPHI Collaboration, Phys. Lett. **B 311** (1993) 408;  
ZEUS Collaboration, JHEP **6** (2010) 009; Erratum, *ibid.* JHEP **10** (2010) 030
- [21] S. Bethke, Euro. Phys. J. **C 64** (2009) 689.
- [22] ATLAS Collaboration, Phys. Lett. **B 716** (2012) 1.
- [23] CMS Collaboration, Phys. Lett. **B 716** (2012) 30.
- [24] D.I. Kazakov, [hep-ph/0012288](https://arxiv.org/abs/hep-ph/0012288).